STRUCTURAL CHEMISTRY

ISSN 2053-2296

Structure and intermolecular interactions of the rare amide–pyridine synthon: a cocrystal of nicotinamide and 2-chloro-3-hydroxypyridine

Oluwatoyin Akerele* and Andreas Lemmerer

Jan Boeyens Structural Chemistry Laboratory, Molecular Sciences Institute, School of Chemistry, University of the Witwatersrand, Private Bag 3, PO Wits, 2050, Johannesburg, South Africa. *Correspondence e-mail: oluwatoyin.akerele@wits.ac.za

Received 1 December 2025
Accepted 11 May 2026

Edited by R. I. Cooper, University of Oxford, United Kingdom

This article is part of the collection *Early Career Scientists in Structural Science*.

Keywords: crystal structure; intermolecular interactions; cocrystal; 2-chloropyridin-3-ol; nicotinamide.

CCDC reference: 2433098

Supporting information: this article has supporting information at journals.iucr.org/c

Nicotinamide (Nico) and derivatives of pyridine are important materials in both the pharmaceutical and agrochemical industries. In the 21st century, pyridine-based agrochemical products achieved commercial success because of their structural diversity and different modes of action that can be explored to improve the effectiveness of the compounds. In this article, we explore the cocrystallization of nicotinamide/isonicotinamide and substituted pyridines and their synthons to understand their ease of formation. A cocrystal of Nico and 2-chloro-3-hydroxypyridine (2Cl3OHPY) was synthesized using solution and mechanochemical methods, and characterized by X-ray diffraction. The structural stability and intermolecular interaction of the (Nico)·(2Cl3OHPY) cocrystal were investigated using differential scanning calorimetry (DSC) and density functional theory (DFT). The cocrystal has strong chain (N—H···N), dimer (N—H···O) and discrete (N—H···O) hydrogen bonds with energy strengths of −31.21, −66.99 and −36.82 kJ mol^{-1}, respectively, and a short C—H···π bond that builds a twisted three-dimensional structure (viewed along the *c* axis) and stabilizes the crystal packing. The results show that the compound is chemically stable, and the two dominating interactions are electrostatic and dispersion energies. An analysis of the aromatic amide and pyridine synthon in the CSD reveals the presence of close supporting interactions that strengthen the N—H···N hydrogen bond. The understanding of the structural properties and intermolecular interactions in the (Nico)·(2Cl3OHPY) cocrystal and $NH_2\cdots N_{py}$ synthon provided in this study could be used to design materials for different applications, including pigments, explosives, drugs, agrochemicals and food additives.

1. Introduction

Cocrystallization is a technique that is used in different fields, such as pharmaceuticals, agrochemicals and materials science, to improve the properties of compounds and design materials with desired properties (Dutt *et al.*, 2021). The strategy for designing cocrystals incorporates the chemical identity of the components, the intermolecular interactions and the crystallization method. A cocrystal is a multi-component crystal containing two or more neutral molecules in a definite stoichiometric ratio; it is formed primarily through strong hydrogen-bonding interactions and has a unique structure and properties compared to the single components (Bond, 2011). Amide and pyridine functional groups are commonly found in many pharmaceutical and agrochemical active ingredients (Mohabbat *et al.*, 2024; Ling *et al.*, 2021; Diniz *et al.*, 2018). In fact, pyridine-based agrochemical products have achieved commercial success in the 21st century because of their structural diversity and different modes of action that can be

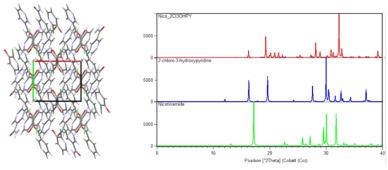

Table 1
The average value of the hydrogen-bond length of the two synthons.

Synthon	Hydrogen bond	Lower quartile	Upper quartile	Average	Standard deviation
Acid–pyridyl synthon	H···*A* (Å)	1.68	1.84	1.77	0.19
	D···*A* (Å)	2.60	2.68	2.65	0.08
Amide–pyridyl synthon	H···*A* (Å)	2.14	2.36	2.26	0.18
	D···*A* (Å)	2.98	3.12	3.00	0.05

explored to improve the effectiveness of the compounds (Zakharychev & Martsynkevich, 2024; Wang *et al.*, 2025; Guan *et al.*, 2016). These pyridyl molecules also cocrystallize with other compounds through noncovalent interactions to form cocrystals or salts. However, the amide–pyridine synthon has the least probability of occurrence in the Cambridge Structural Database (CSD; Groom *et al.*, 2016) when compared with both homosynthons and heterosynthons of acid, amide and pyridine functional groups (Babu *et al.*, 2007). In fact, a search of the CSD in June 2025 revealed the number of amide and pyridyl synthons to be less than 10% of carboxylic acid and pyridyl synthons (Bruno *et al.*, 2002).

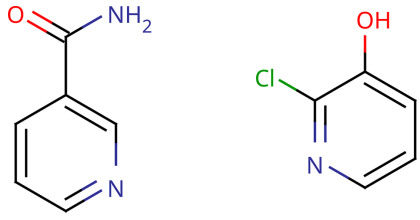

(Nico)·(2Cl3OHPY)
Scheme 1

Similarly, a specific search for nicotinamide or isonicotinamide and pyridine derivatives yields less than 20 hits in the CSD. Studies have analyzed the synthons and interactions between OH···N_{py} and COOH···N_{py} (Lemmerer *et al.*, 2013; Bis *et al.*, 2007; Shattock *et al.*, 2008; Ganie *et al.*, 2022; Goswami *et al.*, 2016; Kavuru *et al.*, 2010; Sharma *et al.*, 2022; Ngoma Tchibouanga & Jacobs, 2020; Sowmya & Kumar, 2023; Jarzembska *et al.*, 2017; Kusuma *et al.*, 2022), but there is no study, to the best of our knowledge, that has examined the NH_2···N_{py} synthon, its structure and interactions. On this note, we conducted a systematic set of cocrystallization experiments on nicotinamide/isonicotinamide and a series of pyridine derivatives using both solution and mechanochemical methods to understand the ease of formation, structure and intermolecular interactions of the multi-component crystals. There was, however, only one success, and so this study has focused on the analysis of the structure and intermolecular interactions of the cocrystal formed by nicotinamide (Nico) and 2-chloro-3-hydroxypyridine (2Cl3OHPY) (Scheme 1), as well as the related structures (NH_2···N_{py} synthon) in the CSD. The pattern revealed in this study could be used to design novel materials and influence the building of a predefined crystal network.

2. Experimental

2.1. *Conquest* search

A search for carboxylic acid and the pyridyl ring, including a H···N contact, in the CSD, with filters for 3D coordinates determined and only organics, gave 2661 hits. The search for amide and the pyridyl ring with the same filters gave only 161 hits, which is less than 10% of the former, as shown in Fig. 1.

The average hydrogen-bond distance in COOH···N_{py} is much lower than in $CONH_2$···N_{py}, as shown in Table 1. This suggests that the hydrogen-bond strength of COOH···N_{py} is stronger than the $CONH_2$···N_{py} hydrogen bond, which correlates with the literature. The strength of the interaction energy of the amide–pyridine synthons is one of the factors contributing to their low occurrence in the CSD. Since there is a connection between the molecular structure and the crystal structure formed (Nangia & Desiraju, 1999), analysis of the structure and interactions (both strong and weak bonds) of the new cocrystal and related architecture will provide an insight into the factors that control the crystal packing.

Analysis of the 161 hits (amide and pyridyl synthon) reviews the proportion for which the NH_2···N_{py} hydrogen bonds occur in the CSD: 50 hits are seen in a component crystal that has both pyridyl ring and amide functional groups (for example, refcode LOCSOP; Dyachenko *et al.*, 2023), 62

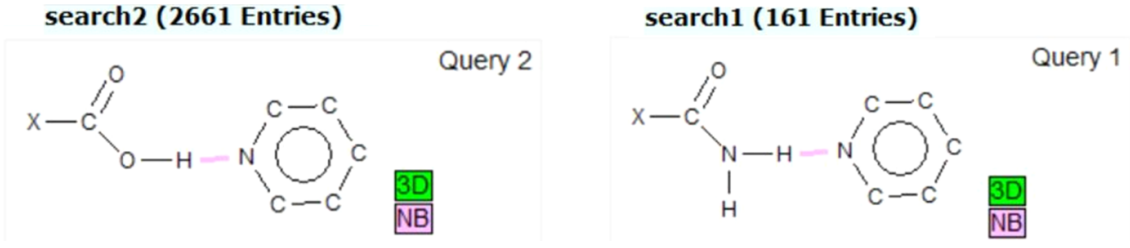

Figure 1
The query fragment for the synthon search.

Table 2
Crystal structures in the CSD with aromatic amide–pyridyl synthons along their bond angles and interaction energy ($NH_2\cdots N_{py}$).

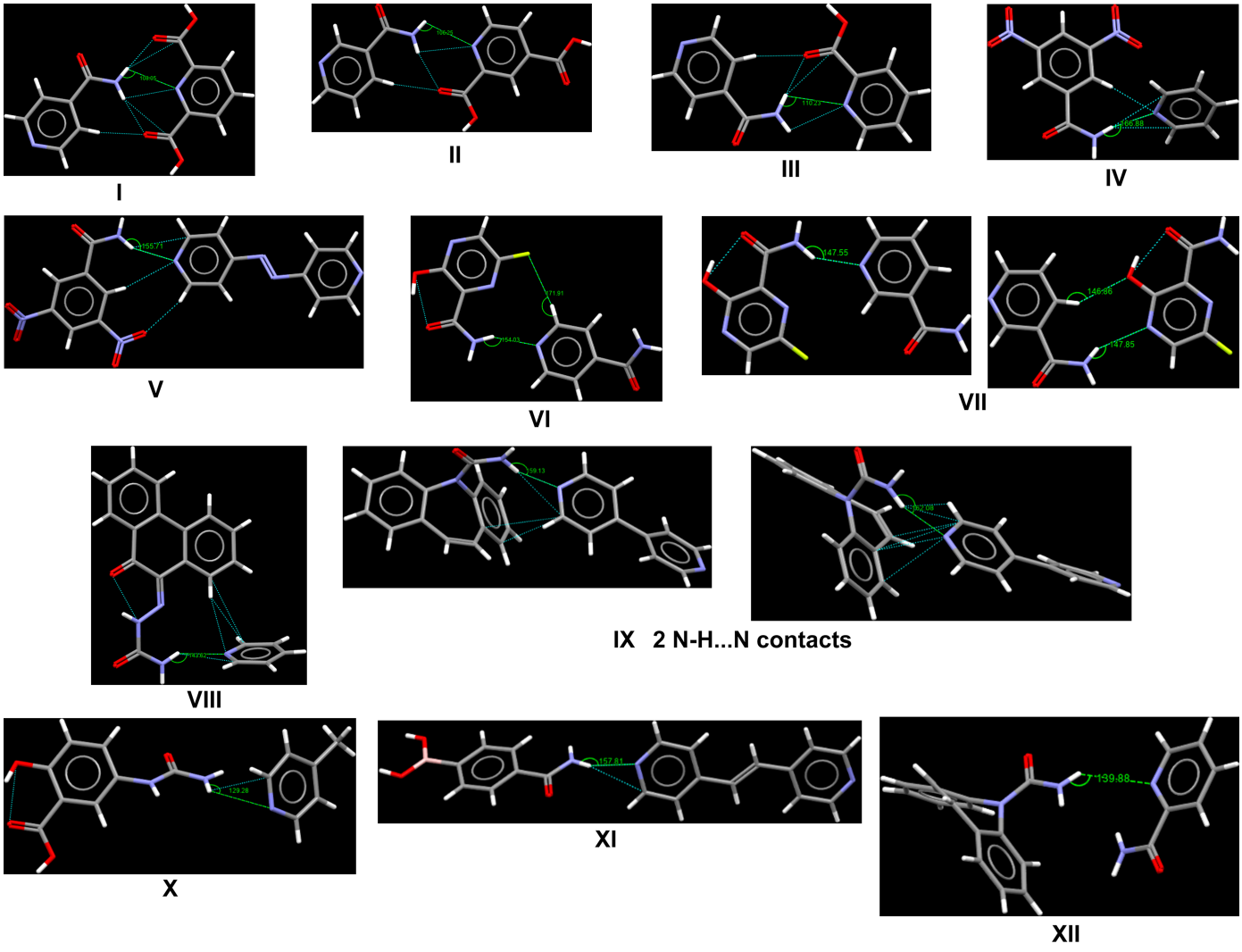

No.	CSD refcode	Reference	Bond angle (°)	Interaction energy (kJ mol^{-1})
I	MELYEI	Aghabozorg *et al.* (2006)	108	−54.48
II	LOTTEX	Ezekiel *et al.* (2024)	106	−43.30
III	PAQMIG	Ganduri *et al.* (2017)	110	−42.84
IV	CAYJIW	Arora *et al.* (2005)	167	−47.61
V	BULJOJ	Ravat *et al.* (2015)	156	−41.84
VI	KOHPUW	Wong *et al.* (2024)	154	−33.43
VII	QOQNUJ	Li *et al.* (2024)	148	−26.48
			148	−25.19
VIII	KUVYOR	Walshe *et al.* (2015)	144	−31.34
IX	XAQQUC	McMahon *et al.* (2005)	159	−30.46
	(2 N—H···N contacts)		162	−34.81
X	IVORUI	Kennedy *et al.* (2016)	129	−25.15
XI	QUGRIX	Barba Hernández *et al.* (2024)	159	−24.48
XII	DOSDOI	Boycov *et al.* (2024)	140	−14.14

hits occur between nicotinamide or isonicotinamide in a component and multi-component environments [KIPGUO (Surov *et al.*, 2022) and JEDHOT (Li *et al.*, 2018)] and 49 are found between two components of pyridyl and amide molecules. There is an even distribution among these groups, which suggests that the amide–pyridyl hydrogen bond will form irrespective of its environment. An analysis of the subset of 49 hits shows that 70% were between aliphatic amides (formamide and urea) and pyridyl molecules, while 30% were between aromatic amides and pyridyl molecules.

2.1.1. Analysis of the aromatic $NH_2\cdots N_{py}$ synthon and structures in the CSD

– The crystal structures with aromatic amide–pyridyl synthons along with their bond angles and interaction energies are shown in Table 2. The average interaction energy (calculated using *GAUSSIAN16*, B3LYP/def2-TZVP; Frisch *et al.*, 2016) of the $NH_2\cdots N_{py}$ bond is −33.26 kJ mol^{-1}.

– The bond angles do not correlate with the interaction energy; for instance, compounds with carbonyl groups at positions 2 and 6 of a pyridyl ring has low angles but strong interaction energies (see structures I–III). Conversely, bulky compounds with two or more phenyl rings have high angles but weak interaction energy (see structures VIII, IX, XI and XII). However, it should be noted that structures IV–VII show correlation between the bond angle and interaction energy. Therefore, the bond angles should be used with care to determine the strength of the bond between the aromatic amide and pyridyl cocrystallization components.

– Analysis of the structure and interactions of aromatic amide–pyridyl synthons reveals the functional groups and additional supporting interactions closer to the $NH_2\cdots N_{py}$ bond as factors influencing the strength of the bond. For instance, the presence of carboxylic acid groups at positions 2 and 5 of pyridine strengthens the $NH_2\cdots N_{py}$ bond, as seen in structures I–III. However, there is approximately a −13 kJ mol^{-1} reduction in energy when there is only one carboxylic group at position 2 or 5, as seen in structures II and III. Structures IV and V have a nitro group at positions 3 and 5 of the aromatic amides and the supporting interaction (C—H$\cdots$N) contributes to the strength of the $NH_2\cdots N_{py}$ bond. On the other hand, with the presence of hydroxyl and fluorine groups at positions 3 and 5 of the aromatic amide, the bonds formed in structures VI and VII do not improve the strength of the $NH_2\cdots N_{py}$ bond. Similarly, a C—H$\cdots\pi$ supporting interaction in structures VIII–IX does not lead to an appreciable increase in the interaction energy of the $NH_2\cdots N_{py}$ bond. The interaction energy of the $NH_2\cdots N_{py}$ bond in structures X–XII is quite low; this could be due to the absence of a strong supporting interaction closer to the $NH_2\cdots N_{py}$ bond.

– It should be noted that these observations are drawn from a small set of aromatic amide–pyridyl synthons and other factors beyond the interest of this study could be contributing to its low occurrence in the CSD.

2.2. Synthesis

The selected chemicals in Table 3 were purchased from Sigma–Aldrich and used without further purification as received. The crystallizations were carried out using the two common crystal growth methods: slow (solvent) evaporation and mechanochemical.

2.2.1. Slow evaporation method

20 mg of nicotinamide or isonicotinamide was dissolved in 1.5 ml of ethanol and an appropriate molar ratio of the substituted pyridine was added slowly to the prepared solution to give a 1:1 molar ratio and concentrations of 0.11 *M*. The solution was heated and stirred gently on a hotplate at a low temperature of about 30 °C until the compound dissolved completely. The heated solution was cooled to room temperature before the vial was covered with a perforated Parafilm sheet to allow for the evaporation of the solvents. Crystals formed within 5 d and the morphology of the crystals was examined visually under a microscope. A suitably sized crystal of the complex was carefully selected for single-crystal X-ray diffraction (SC-XRD) to ascertain the formation of a multi-component crystal. Powder X-ray diffraction (PXRD) and differential scanning calorimetry (DSC) were also used to analyze the crystals.

Table 3
Selected substituted pyridines for cocrystallization with either nicotinamide or isonicotinamide.

	Substituted pyridine
Nicotinamide or isonicotinamide	Pyridine
	2-Aminopyridine
	3-Aminopyridine
	4-Aminopyridine
	2-Hydroxypyridine
	3-Hydroxypyridine
	4-Hydroxypyridine
	2-Amino-3-nitropyridine
	2-Amino-5-nitropyridine
	2-Amino-5-methylpyridine
	2-Amino-5-chloropyridine
	2-Amino-3-hydroxypyridine
	2-Chloro-3-hydroxypyridine
	3-Amino-2-chloropyridine
	4-Cyanopyridine

2.2.2. Mechanochemical method

80 mg of nicotinamide/isonicotinamide and the equivalent 1:1 molar ratio of the substituted pyridine were weighed into a 1.5 ml plastic vial with one stainless steel ball of 4 mm diameter and 10 drops of ethanol. The vials were placed in an adapter for six reactions, and the slurry grinding experiment was carried out in a Retsch MM 400 Mixer Mill at room temperature. The loaded vials were shaken in the Mixer Mill for 60 min at 25 rpm^{-1} or Hz frequency. PXRD analysis was conducted after the resulting powder was dried at 50 °C in an oven. However, there was no new phase formation in all the ground crystallization experiments except for the (Nico)·(2-Cl3OHPY) cocrystal. The PXRD results for the unsuccessful cocrystals with the starting materials are given in the supporting information.

2.3. Refinement

Crystal data, data collection and structure refinement details are summarized in Table 4. All atoms were refined anisotropically before the inclusion of H atoms. H atoms on aromatic rings were placed in calculated positions, while the sp^3-hybridized C atoms were derived from electron-density maps. The H atom on the N atom was also derived from an electron-density difference map and refined freely. All images,

including the crystal packing, were created using *Mercury* (Macrae *et al.*, 2020).

2.4. Powder X-ray diffraction (PXRD)

PXRD was used to further confirm the formation of the new cocrystal. A diffractogram of a powdered crystalline sample of the multi-component crystal was measured at 293 K using a Bruker D2 phaser powder X-ray diffractometer. The instrument is equipped with a sealed tube Co $K\alpha_1$ X-ray source (λ = 1.78896 Å) and a LynxEye PSD detector in Bragg–Brentano geometry, and operating at 30 kV and 10 mA. The data collection was carried out with a scanning interval ranging from 2θ = 5.0015 to 40° at a scan speed of 0.5 s per step (with an increment step size of 0.028445°). The experimental and simulated powder pattern of the new cocrystal is given in the supporting information. The overlay of the simulated patterns presented in Fig. 2 shows the different intensity peaks for nicotinamide, 2-chloro-3-hydroxypyridine and the (Nico)·(2-Cl3OHPY) cocrystal.

2.5. Thermal analysis

Differential scanning calorimetry (DSC) was used to measure the change in the heat flow of the sample as temperature changes (Newman & Wenslow, 2018). The sample was heated and cooled to determine the melting points, enthalpies of phase transitions and stability of any different phases. The temperature and energy calibrations were performed using pure indium (purity 99.99%, m.p. 156.6 °C, heat of fusion 28.45 J g^{-1}) and pure zinc (purity 99.99%, m.p. 419.5 °C, heat of fusion 112 J g^{-1}). A Mettler Toledo DSC 3 was used to collect the DSC data and aluminium pans were placed under nitrogen gas at a flow rate of 10 ml min^{-1}. At a heating or cooling rate of 10 °C min^{-1}, the samples were heated from 25 °C to the final temperature, which is the temperature just after the sample melting point, as visually established from the hot stage, and then cooled to 25 °C. The exothermic peak, which is the amount of heat (energy) released as the temperature changes, was used to determine the thermal stability of the multi-component crystal. The plot of the DSC thermogram for the (Nico)·(2Cl3OHPY) is given in Fig. 3.

Table 4
Experimental details.

Crystal data	
Chemical formula	$C_6H_6N_2O{\cdot}C_5H_4ClNO$
M_r	251.67
Crystal system, space group	Monoclinic, $P2_1/n$
Temperature (K)	173
a, b, c (Å)	8.0095 (3), 6.6434 (2), 20.6585 (6)
β (°)	92.563 (1)
V (Å^3)	1098.15 (6)
Z	4
Radiation type	Mo $K\alpha$
μ (mm^{-1})	0.34
Crystal size (mm)	0.20 × 0.15 × 0.09
Data collection	
Diffractometer	Bruker APEXII CCD
No. of measured, independent and observed [$I > 2\sigma(I)$] reflections	19834, 2745, 2461
R_{int}	0.041
$(\sin\theta/\lambda)_{max}$ (Å^{-1})	0.671
Refinement	
$R[F^2 > 2\sigma(F^2)]$, $wR(F^2)$, S	0.032, 0.091, 1.06
No. of reflections	2745
No. of parameters	155
H-atom treatment	H-atom parameters constrained
$\Delta\rho_{max}$, $\Delta\rho_{min}$ (e Å^{-3})	0.33, −0.23

Computer programs: *SAINT* (Bruker, 2021), *APEX4* (Bruker, 2021), *SHELXT2018* (Sheldrick, 2015*a*), *SHELXL2018* (Sheldrick, 2015*b*) and *OLEX2* (Dolomanov *et al.*, 2009).

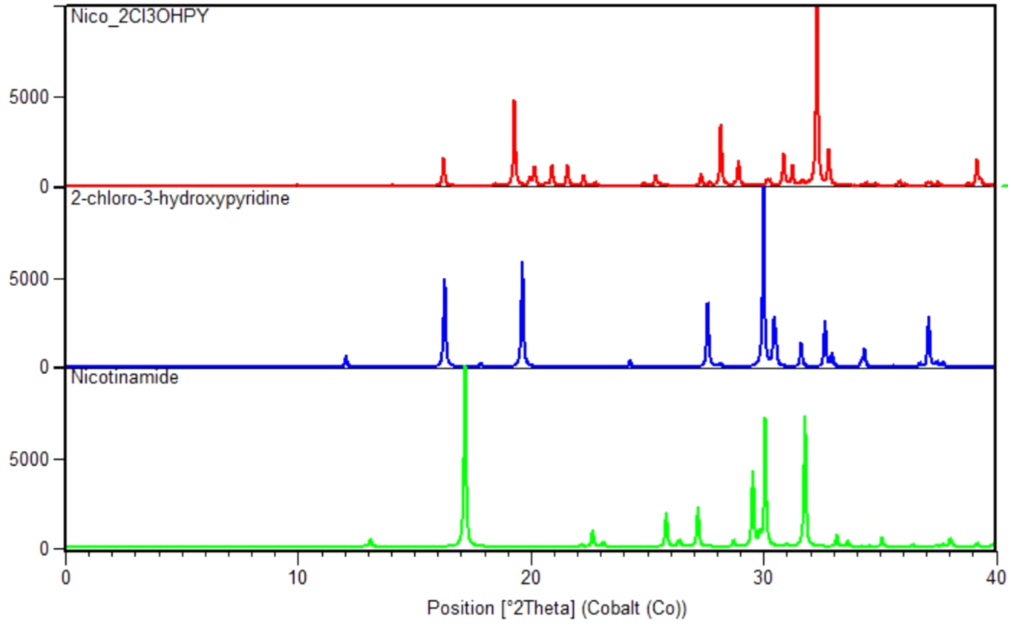

Figure 2
Simulated PXRD patterns: blue is 2-chloro-3-hydroxypyridine, green is nicotinamide and red is the new multi-component cocrystal (Nico)·(2Cl3OHPY).

2.6. Computational studies

2.6.1. Interaction energy between molecules in units in the multi-component crystal

The *GAUSSIAN16* suite of programs was used for the optimization of the H-atom positions with the default Berny algorithm (Frisch *et al.*, 2016; Li & Frisch, 2006). The H-atom positions of the molecular structure obtained from the crystal structures were optimized in the gas phase at the B3LYP functional with the def2-TZVP basis set and incorporate Grimme's D3 dispersion correction for a proper description of the dispersion interactions (Becke, 1997; Becke, 1992; Zhao & Truhlar, 2008; Grimme *et al.*, 2010). The H-atom positions from crystal structures are not accurately determined by X-ray crystallography. This was done to obtain the interaction energy within the two molecules in a unit and was calculated with the same theoretical method (B3LYP-D3/def2-TZVP), taking the basis set superposition error (BSSE) into account with the counterpoise correction (Simon *et al.*, 1996; Boys & Bernardi, 1970; Ransil, 1961). The theoretical details can be found in our previous article (Akerele & Lemmerer, 2025).

Chemcraft (Zhurko, 2026) software was used to analyze and visualize the output generated from *GAUSSIAN16* calculations.

2.6.2. Hirshfeld surfaces and intermolecular interactions

CrystalExplorer (Spackman *et al.*, 2021) was used to generate the Hirshfeld surfaces (HS) at high standard resolution using the CIF as the input file. *CrystalExplorer* creates colour-coded and HS surface maps that help to visualize the important regions of the intermolecular interactions on the surface. The standard normalized contact (d_{norm}) of Hirshfeld surface analysis is given as follows:

$$d_{norm} = \frac{d_i - r_i^{vdW}}{r_i^{vdW}} + \frac{d_e - r_e^{vdW}}{r_e^{vdW}}$$

where d_i is the distance that represents the nucleus inside the surface and d_e is the distance from the HS to the nearest core outside the surface (Dege *et al.*, 2022).

The d_{norm} is the range of distances between the surface and the nearest atomic external surfaces (d_e) and internal surfaces (d_i). Red contacts are those that are shorter than the van der Waals radii (vdW), indicating that the atoms that form intermolecular bonds are closer than the sum of their radii (Garg & Azim, 2022). Contacts with distances equal to the sum of the van der Waals radii are shown on the white surface. A blue colour indicates interactions that are more distinct – that is, contacts that are longer than the sum of the van der Waals radii (Dege *et al.*, 2022; Zeng *et al.*, 2023; Garg & Azim, 2022; Garg *et al.*, 2021; Garg *et al.*, 2022).

CrystalExplorer was also used to calculate the lattice energies of the molecular systems. The wavefunctions of the molecular system were calculated with the built-in *TONTO* program at the CE-B3LYP/6-31G(d,p) theoretical level (Jayatilaka & Grimwood, 2003; Mackenzie *et al.*, 2017; Turner *et al.*, 2015). All the energies of interaction between the selected molecule (at the centre of the cluster) and its neighbouring molecules were computed; the model then separated the total energies into different components, such as electrostatic, polarization, dispersion and repulsion energy components (Spackman *et al.*, 2008).

3. Results and discussion

3.1. Crystallization experiment

The crystallization experiment results between nicotinamide or isonicotinamide and all the substituted pyridines listed in Table 2 were unsuccessful, except for nicotinamide (Nico) and 2-chloro-3-hydroxypyridine (2Cl3OHPY), which gave a cocrystal *via* both crystallization methods. This is the only multi-component cocrystal obtained and was discovered

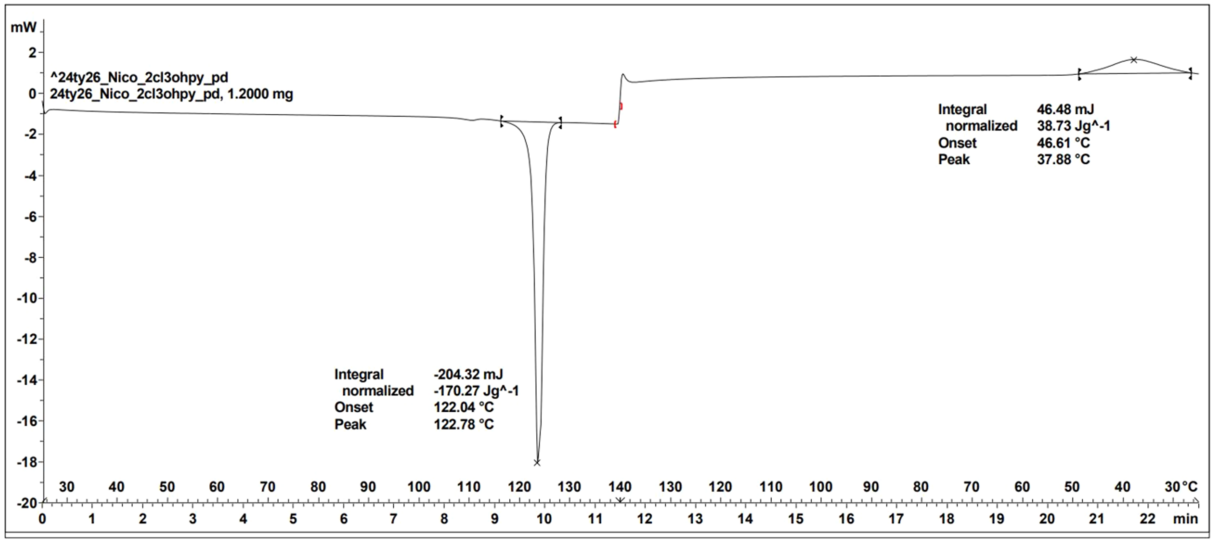

Figure 3
The DSC scan of (Nico)·(2Cl3OHPY).

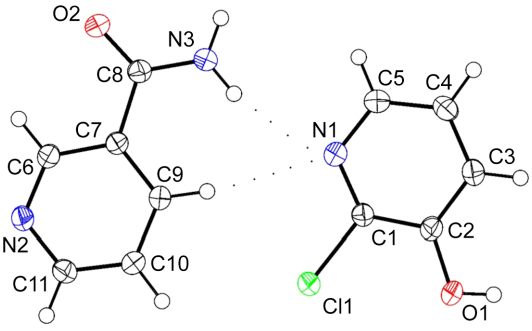

Figure 4
The molecular structure of the cocrystal, showing the atom-numbering scheme of the asymmetric unit. Displacement ellipsoids are drawn at the 50% probability level and H atoms are shown as small spheres of arbitrary radii.

for the first time in this study. The unsuccessful crystallization experiments led to the formation of crystals of each starting material only.

3.2. Molecular structure of (Nico)·(2Cl3OHPY)

The asymmetric unit of multi-component crystal (Nico)·(2Cl3OHPY) is shown in Fig. 4.

3.2.1. Crystal packing of the molecular structure

(Nico)·(2Cl3OHPY) crystallized in the monoclinic space group $P2_1/n$ with $Z' = 2$. Fig. 5 shows the units that drive the packing arrangement of the molecular structure. The asymmetric unit has two symmetry-independent molecules with a discrete $D(2)$ hydrogen bond (Bernstein *et al.*, 1995), through O1—H1···N2 [Fig. 5(*a*)]. Two molecules of nicotinamide related by an inversion operation form a dimer hydrogen bonded with a $R_2^2(8)$ motif through N3—H3*A*···O2^{i} [Fig. 5(*b*)]. The molecules in Fig. 5(*c*) form a chain of hydrogen bonds through N3—H3*B*···N1^{ii}. The asymmetric unit bonds with the nicotinamide through dimer hydrogen bonds in one direction and 2Cl3OHPY through a chain hydrogen bond in another direction in a spiral-like manner along the *c* axis, as shown in Fig. 5(*d*).

The asymmetric units also stack antiparallel and adjacent to one another through short contacts between N3—H3*A*···N2, N3—H3*B*···N1, N1···N2 and Cl1···O2, as shown in Fig. 6(*a*), which resulted in the overall twisted packing arrangement along the *c* axis, as listed in Fig. 6(*b*).

Table 5
Hydrogen-bond geometry (Å, °).

D—H···*A*	*D*—H	H···*A*	*D*···*A*	*D*—H···*A*
O1—H1···N2	0.84	1.80	2.6323 (13)	170
N3—H3*A*···O2^{i}	0.88	2.03	2.8883 (13)	167
N3—H3*B*···N1^{ii}	0.88	2.37	3.2062 (14)	159

Symmetry codes: (i) $-x+1, -y+2, -z+1$; (ii) $x+\frac{1}{2}, -y+\frac{1}{2}, z-\frac{1}{2}$.

3.2.2. Intermolecular hydrogen bonds in the (Nico)·(2-Cl3OHPY) cocrystal

The hydrogen bonds between the two starting components are shown in Table 5.

3.3. Theoretical studies

3.3.1. Energetic properties of the (Nico)·(2Cl3OHPY) structure

The energy of interaction within the asymmetric unit and other units are −31.21, −66.99 and −36.82 kJ mol^{-1} for Figs. 5(*a*), 5(*b*) and 5(*c*), respectively, in the gas phase. The strength of the hydrogen bonds of all three units is strong and contributes to the overall stability of the crystal structure. The N—H···O hydrogen-bonded dimer [Fig. 5(*b*)] contributes −33.50 kJ mol^{-1} per donor, which falls within the discrete and chain hydrogen-bond energy.

A −5 kJ mol^{-1} increase is observed in the interaction energy of Figs. 5(*a*) and 5(*c*); this further indicates that the strength of interaction of O—H···N is stronger than

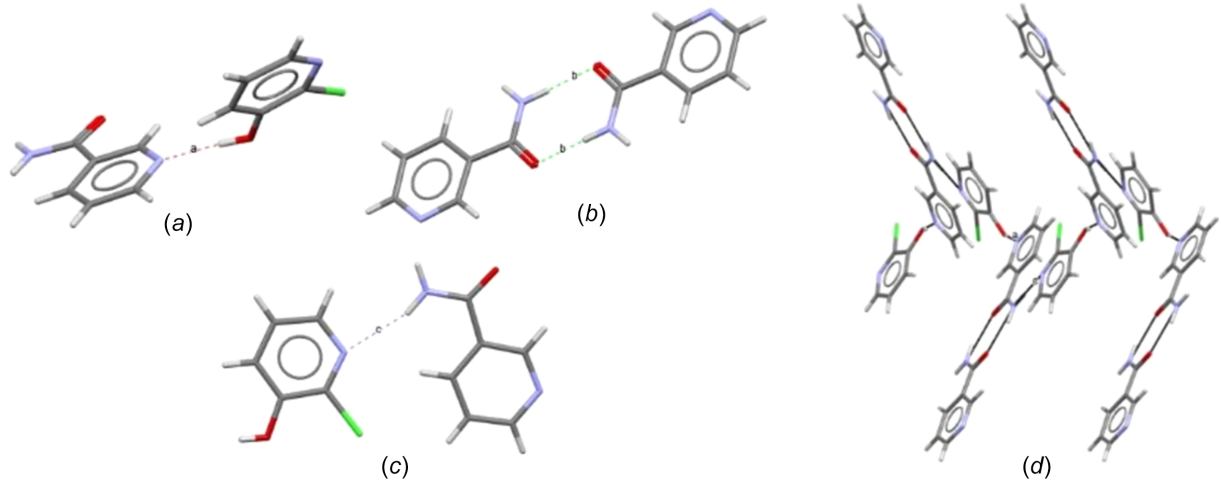

Figure 5
(*a*) The discrete $D(2)$ hydrogen bond, (*b*) the dimer $R_2^2(8)$ hydrogen bond, (*c*) the chain $C(2)$ hydrogen bond and (*d*) the molecules packed in opposite directions in a spiral-like manner along the *c* axis.

N—H···N. This suggests that the strength of energy (hydrogen bond) could be one of the factors that is not favouring the formation of the N—H···N hydrogen bond, alongside the elusive crystallization of nicotinamide/isonicotinamide and substituted pyridine cocrystal, thereby leading to the lower number of amide–pyridyl structures in the CSD.

3.3.2. Hirshfeld surface (HS) analysis of the (Nico)·(2-Cl3OHPY) cocrystal

To visualize the molecular packing and interactions in the crystal structures, a HS analysis was carried out using *CrystalExplorer* (Version 21) (Dege *et al.*, 2022; Spackman & Jayatilaka, 2009).

The HSs and fingerprint plots (FPs) are given in the supporting information (Figs. S7–S11). The HSs show intense red regions for N—H···O hydrogen bonds and light-red regions for C···O and H···H contacts. The FPs show high percentages for the following interactions: H···H 24.5%, O···H/H···O 18.0%, Cl···H/H···Cl 16.2%, C···H/H···C 15.0% and N···H/H···N 10.6%. These results confirm the importance of these interactions in the (Nico)·(2Cl3OHPY) cocrystal.

3.3.3. Interaction energy of the (Nico)·(2Cl3OHPY) crystal structure

The addition of interaction energy calculations in *CrystalExplorer* allows for the precise calculation of the intensity of interactions, which may be directly compared to the outcomes obtained from HS analysis.

The CE-B3LYP/6-31G(d,p) energy model, which is accessible in *CrystalExplorer21* (Turner *et al.*, 2017; Garg *et al.*, 2022; Akhileshwari *et al.*, 2022; Frisch *et al.*, 1984), is used to compute the lattice energy. A cluster of molecules is created by applying crystallographic symmetry operations to a chosen central molecule within a radius of 20 Å (Hirshfeld, 1977). The total energies (E_{tot}) are separated into different components, such as electrostatic (E_{ele}), polarization (E_{pol}), dispersion (E_{dis}) and repulsion (E_{rep}) energies (Chen *et al.*, 2018), with respective scale factors of 1.057, 0.740, 0.871 and 0.618.

The summation of the lattice energy (in kJ mol^{-1}) for the (Nico)·(2Cl3OHPY) structure is −66.750 (E_{ele}), −14.097 (E_{pol}), −64.650 (E_{dis}), 58.138 (E_{rep}) and −87.358 kJ mol^{-1} (E_{tot}) for N—H···O. The evaluation of the energy components shows that the electrostatic and dispersion energies are the highest contributors to the stability of the structure. This suggests that hydrogen bonds and other noncovalent interactions are contributing to the stability of the (Nico)·(2-Cl3OHPY) crystal structure.

4. Discussion

The present study combines a series of substituted pyridines with nicotinamide and isonicotinamide using two common crystal growth methods; however, only one cocrystal was obtained. The crystal structure, (Nico)·(2Cl3OHPY), has strong O—H···N, N—H···O and N—H···N hydrogen bonds, and weak noncovalent interactions that stabilize and drive the twisted three-dimensional packing arrangement along the *c* axis. The interaction energy of the $NH_2\cdots N_{py}$ hydrogen bond is −31.21 kJ mol^{-1}, and is supported by a close interaction between the C—H···N hydrogen bond. The FP and HSs confirm the importance of these interactions (O···H/H···O 18.0%, C···H/H···C 15.0% and N···H/H···N 10.6%) relative to other intermolecular interactions. The DSC result for the enthalpy of fusion of the compound in its pure phase is 42.852 kJ mol^{-1}, which is an indication of the thermodynamic stability of the cocrystal form. The cocrystal is thermodynamically stable, with a sum energy of −103.255 kJ mol^{-1}, and the two dominating interactions are electrostatic and dispersion energies.

The analysis of the crystal structures in the CSD shows that the average bond distance in $CONH_2\cdots N_{py}$ is greater than in $COOH\cdots N_{py}$. The investigation of the $NH_2\cdots N_{py}$ synthon

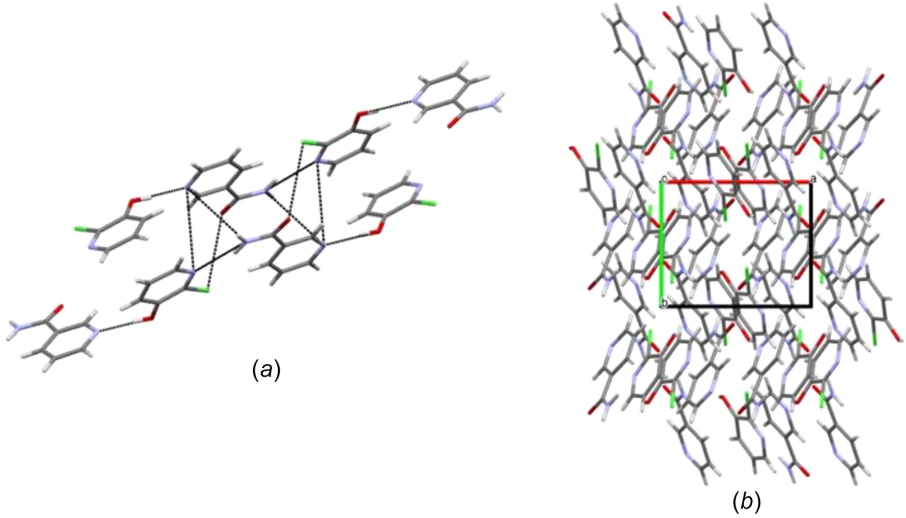

Figure 6
(*a*) The noncovalent interactions joining adjacent chains [symmetry code: (i) $x+\frac{1}{2}, -y+\frac{1}{2}, z-\frac{1}{2}$]. (*b*) The overall packing arrangement along the *b* axis.

and interactions in the CSD reveals a higher occurrence of the $NH_2\cdots N_{py}$ synthon in two similar molecules and aliphatic amide–pyridyl than in aromatic amide–pyridyl systems (Chen *et al.*, 2018; Aakeröy *et al.*, 2011). Furthermore, the strength of the aromatic $NH_2\cdots N_{py}$ bond does not correlate with the bond angles, and the strength of the $NH_2\cdots N_{py}$ bond is observed to be influenced by the presence of close supporting interactions and functional groups, such as carboxylic acid and nitro groups. This suggests, amongst other things, why there are not many examples of the $NH_2\cdots N_{py}$ synthon in the CSD.

Crystal engineers rely on the control of directional interactions and synthons in the assembly of functional materials (Desiraju, 2011). These strong hydrogen bonds are important in the initial stage of molecular aggregation; however, weak interactions are equally important in the molecular packing at the final stage of assemblies and can induce crystal packing variations (Desiraju, 2013; Ravat *et al.*, 2015).

5. Conclusions

This study conducted the synthesis of a cocrystal of nicotinamide (Nico) and 2-chloro-3-hydroxypyridine (2Cl3OHPY) and analyzed the structural properties and intermolecular interaction of the product using both experimental and computational methods. The study also reveals the trends in the occurrence of the $NH_2\cdots N_{py}$ synthon in the CSD. Understanding the structural properties and intermolecular interactions in the (Nico)·(2Cl3OHPY) cocrystal provided in this study contributed to the molecular recognition of the amide–pyridyl cocrystal.

The functional groups, close interactions and other insights generated from this study could be harnessed to potentially predict the cocrystallization of amide–pyridyl systems.

Acknowledgements

Funding for this research was provided by the University of the Witwatersrand, Johannesburg (Research office).

References

Aakeröy, C. B., Chopade, P. D. & Desper, J. (2011). *Cryst. Growth Des.* **11**, 5333–5336.
Aghabozorg, H., Ghadermazi, M. & Attar Gharamaleki, J. (2006). *Acta Cryst.* E**62**, o3445–o3447.
Akerele, O. & Lemmerer, A. (2025). *Acta Cryst.* C**81**, 310–318.
Akhileshwari, P., Sharanya, K. & Sridhar, M. A. (2022). *J. Chem. Crystallogr.* **52**, 324–336.
Arora, K. K., PrakashaReddy, J. & Pedireddi, V. R. (2005). *Tetrahedron* **61**, 10793–10800.
Babu, N. J., Reddy, L. S. & Nangia, A. (2007). *Mol. Pharm.* **4**, 417–434.
Barba Hernández, M., Vasquez-Rios, M. G., Hopfl, H. & Macgillivray, L. R. (2024). *Cryst. Growth Des.* **25**, 38–52.
Becke, A. D. (1992). *J. Chem. Phys.* **96**, 2155–2160.
Becke, A. D. (1997). *J. Chem. Phys.* **107**, 8554–8560.
Bernstein, J., Davis, R. E., Shimoni, L. & Chang, N. L. (1995). *Angew. Chem. Int. Ed. Engl.* **34**, 1555–1573.
Bis, J. A., Vishweshwar, P., Weyna, D. & Zaworotko, M. J. (2007). *Mol. Pharm.* **4**, 401–416.
Bond, A. D. (2011). *Fundamental aspects of salts and cocrystals*, in *Pharmaceutical Salts and Co-crystals*, ch. 2, pp. 9–28. Cambridge: The Royal Society of Chemistry.
Boycov, D. E., Drozd, K. V., Manin, A. N., Churakov, A. V. & Perlovich, G. L. (2024). *Cryst. Growth Des.* **24**, 4862–4873.
Boys, S. F. & Bernardi, F. J. M. P. (1970). *Mol. Phys.* **19**, 553–566.
Bruker (2021). *APEX4*, *SAINT* and *SADABS*. Bruker AXS Inc., Madison, Wisconsin, USA.
Bruno, I. J., Cole, J. C., Edgington, P. R., Kessler, M., Macrae, C. F., McCabe, P., Pearson, J. & Taylor, R. (2002). *Acta Cryst.* B**58**, 389–397.
Chen, C., Zhang, K., Sun, Y., Xiang, S., Geng, Y., Liu, K. & Wang, L. (2018). *J. Mol. Struct.* **1170**, 60–69.
Dege, N., Gökce, H., Doğan, O. E., Alpaslan, G., Ağar, T., Muthu, S. & Sert, Y. (2022). *Colloids Surf. A Physicochem. Eng. Asp.* **638**, 128311.
Desiraju, G. R. (2011). *Cryst. Growth Des.* **11**, 896–898.
Desiraju, G. R. (2013). *J. Am. Chem. Soc.* **135**, 9952–9967.
Diniz, L. F., Souza, M. S., Carvalho, P. S. Jr, da Silva, C. C., D'Vries, R. F. & Ellena, J. (2018). *J. Mol. Struct.* **1153**, 58–68.
Dolomanov, O. V., Bourhis, L. J., Gildea, R. J., Howard, J. A. K. & Puschmann, H. (2009). *J. Appl. Cryst.* **42**, 339–341.
Dutt, B., Choudhary, M. & Budhwar, V. (2021). *Drug. Deliv. Lett.* **11**, 136–155.
Dyachenko, I. V. V. D., Dyachenko, P. V., Dorovatovskii, V. N., Khrustalev, V. N. & Nenajdenko, V. G. (2023). *Russ. J. Org. Chem.* **59**, 1158–1170.
Ezekiel, C. I., Jadhav, S., Stevens, L. L. & MacGillivray, L. R. (2024). *Cryst. Growth Des.* **24**, 6618–6624.
Frisch, M. J., Pople, J. A. & Binkley, J. S. (1984). *J. Chem. Phys.* **80**, 3265–3269.
Frisch, M. J., Trucks, G. W., Schlegel, H. B., Scuseria, G. E., Robb, M. A., Cheeseman, J. R., Scalmani, G., Barone, V., Mennucci, B., Petersson, G. A., Nakatsuji, H., Caricato, M., Li, X., Hratchian, H. P., Izmaylov, A. F., Bloino, J., Zheng, G., Sonnenberg, J. L., Hada, M., Ehara, M., Toyota, K., Fukuda, R., Hasegawa, J., Ishida, M., Nakajima, T., Honda, Y., Kitao, O., Nakai, H., Vreven, T., Montgomery, J. A., Peralta, J. E., Ogliaro, F., Bearpark, M., Heyd, J. J., Brothers, E., Kudin, K. N., Staroverov, V. N., Kobayashi, R., Normand, J., Raghavachari, K., Rendell, A., Burant, J. C., Iyengar, S. S., Tomasi, J., Cossi, M., Rega, N., Millam, J. M., Klene, M., Know, J. E., Cross, J. B., Bakken, V., Adamo, C., Jaramillo, J., Gomperts, R., Stratmann, R. E., Yazyev, O. A., Austin, J., Cammi, R., Pomelli, C., Ochterski, J. O., Martin, R. L., Morokuma, K., Zakrzweski, V. G., Voth, G. A., Salvador, P., Dannenberg, J. J., Dapprich, S., Daniels, A. D., Farkas, O., Foresman, J. B., Ortiz, J. V., Cioslowski, J. & Fox, D. J. (2016). *GAUSSIAN16*. Revision C.01. Gaussian Inc., Wallingford, CT, USA. https://gaussian.com/.
Ganduri, R., Cherukuvada, S., Sarkar, S. & Guru Row, T. N. (2017). *CrystEngComm* **19**, 1123–1132.
Ganie, A. A., Rashid, S., Ahangar, A. A., Ismail, T. M., Sajith, P. K. & Dar, A. A. (2022). *Cryst. Growth Des.* **22**, 1972–1983.
Garg, U. & Azim, Y. (2022). *J. Mol. Struct.* **1269**, 133820.
Garg, U., Azim, Y. & Alam, M. (2021). *RSC Adv.* **11**, 21463–21474.
Garg, U., Azim, Y., Alam, M., Kar, A. & Pradeep, C. P. (2022). *Cryst. Growth Des.* **22**, 4316–4331.
Goswami, P. K., Thaimattam, R. & Ramanan, A. (2016). *Cryst. Growth Des.* **16**, 1268–1281.
Grimme, S., Antony, J., Ehrlich, S. & Krieg, H. (2010). *J. Chem. Phys.* **132**, 154104.
Groom, C. R., Bruno, I. J., Lightfoot, M. P. & Ward, S. C. (2016). *Acta Cryst.* B**72**, 171–179.
Guan, A. Y., Liu, C. L., Sun, X. F., Xie, Y. & Wang, M. A. (2016). *Bioorg. Med. Chem.* **24**, 342–353.
Hirshfeld, F. L. (1977). *Theor. Chim. Acta* **44**, 129–138.
Jarzembska, K. N., Hoser, A. A., Varughese, S., Kamiński, R., Malinska, M., Stachowicz, M., Pedireddi, V. R. & Woźniak, K. (2017). *Cryst. Growth Des.* **17**, 4918–4931.

Jayatilaka, D. & Grimwood, D. J. (2003). *TONTO: a fortran based object-oriented system for quantum chemistry and crystallography*, in *International Conference on Computational Science*, pp. 142–151. Berlin, Heidelberg: Springer Berlin Heidelberg.
Kavuru, P., Aboarayes, D., Arora, K. K., Clarke, H. D., Kennedy, A., Marshall, L., Ong, T. T., Perman, J., Pujari, T., Wojtas, Ł. & Zaworotko, M. J. (2010). *Cryst. Growth Des.* **10**, 3568–3584.
Kennedy, S. R., Miquelot, A., Aguilar, J. A. & Steed, J. W. (2016). *Chem. Commun.* **52**, 11846–11849.
Kusuma, A. P., Soewandhi, S. N., Mauludin, R., Suendo, V., Kurniawan, F., Pamungkas, G. & Nugraha, Y. P. (2022). *Open Chem.* **20**, 949–957.
Lemmerer, A., Adsmond, D. A., Esterhuysen, C. & Bernstein, J. (2013). *Cryst. Growth Des.* **13**, 3935–3952.
Li, H., Wang, L., Ye, X., Yao, C., Song, S., Qu, Y., Jiang, J., Wang, H., Han, P., Liu, Y. & Tao, X. (2024). *J. Am. Chem. Soc.* **146**, 11592–11598.
Li, M., Li, Z., Zhang, Q., Peng, B., Zhu, B., Wang, J. R., Liu, L. & Mei, X. (2018). *Cryst. Growth Des.* **18**, 6123–6132.
Li, X. & Frisch, M. J. (2006). *J. Chem. Theory Comput.* **2**, 835–839.
Ling, Y., Hao, Z. Y., Liang, D., Zhang, C. L., Liu, Y. F. & Wang, Y. (2021). *Drug. Des. Dev. Ther.* **15**, 4289–4338.
Mackenzie, C. F., Spackman, P. R., Jayatilaka, D. & Spackman, M. A. (2017). *IUCrJ* **4**, 575–587.
Macrae, C. F., Sovago, I., Cottrell, S. J., Galek, P. T. A., McCabe, P., Pidcock, E., Platings, M., Shields, G. P., Stevens, J. S., Towler, M. & Wood, P. A. (2020). *J. Appl. Cryst.* **53**, 226–235.
McMahon, J. A., Bis, J. A., Vishweshwar, P., Shattock, T. R., McLaughlin, O. L. & Zaworotko, M. J. (2005). *Z. Kristallogr. Cryst. Mater.* **220**, 340–350.
Mohabbat, A., Salama, J., Seiffert, P., Boldog, I. & Janiak, C. (2024). *Crystals* **14**, 811.
Nangia, A. & Desiraju, G. R. (1999). *Supramolecular synthons and pattern recognition*, in *Design of Organic Solids*, pp. 57–95. Berlin, Heidelberg: Springer Berlin Heidelberg.
Newman, A. & Wenslow, R. (2018). *Pharmaceutical Crystals: Science and Engineering*, edited by T. Li & A. Mattei, pp. 89–121. Hoboken: John Wiley & Sons Inc.
Ngoma Tchibouanga, R. R. & Jacobs, A. (2020). *J. Mol. Struct.* **1204**, 127195.
Ransil, B. J. (1961). *J. Chem. Phys.* **34**, 2109–2118.
Ravat, P., SeethaLekshmi, S., Biswas, S. N., Nandy, P. & Varughese, S. (2015). *Cryst. Growth Des.* **15**, 2389–2401.
Sharma, P., Gomila, R. M., Frontera, A., Barcelo-Oliver, M. & Bhattacharyya, M. K. (2022). *Crystals* **12**, 1442.
Shattock, T. R., Arora, K. K., Vishweshwar, P. & Zaworotko, M. J. (2008). *Cryst. Growth Des.* **8**, 4533–4545.
Sheldrick, G. M. (2015*a*). *Acta Cryst.* A**71**, 3–8.
Sheldrick, G. M. (2015*b*). *Acta Cryst.* C**71**, 3–8.
Simon, S., Duran, M. & Dannenberg, J. J. (1996). *J. Chem. Phys.* **105**, 11024.
Sowmya, A. & Kumar, G. A. (2023). *Mater. Today: Proc.* **89**, 30–40.
Spackman, M. A. & Jayatilaka, D. (2009). *CrystEngComm* **11**, 19–32.
Spackman, M. A., McKinnon, J. J. & Jayatilaka, D. (2008). *CrystEngComm* **10**, 377–388.
Spackman, P. R., Turner, M. J., McKinnon, J. J., Wolff, S. K., Grimwood, D. J., Jayatilaka, D. & Spackman, M. A. (2021). *J. Appl. Cryst.* **54**, 1006–1011.
Surov, A. O., Voronin, A. P., Drozd, K. V., Volkova, T. V., Vasilev, N., Batov, D., Churakov, A. V. & Perlovich, G. L. (2022). *Cryst. Growth Des.* **22**, 2569–2586.
Turner, M. J., McKinnon, J. J., Wolff, S. K., Grimwood, D. J., Spackman, P. R., Jayatilaka, D. & Spackman, M. A. (2017). *CrystalExplorer17*. University of Western Australia. http://hirshfeld-surface.net.
Turner, M. J., Thomas, S. P., Shi, M. W., Jayatilaka, D. & Spackman, M. A. (2015). *Chem. Commun.* **51**, 3735–3738.
Walshe, N., Crushell, M., Karpinska, J., Erxleben, A. & McArdle, P. (2015). *Cryst. Growth Des.* **15**, 3235–3248.
Wang, S., Chen, Z., Li, S., Fang, H., Chang, J., Yan, X., Gong, Y., Zhang, W. & Hua, X. (2025). *J. Agric. Food Chem.* **73**, 4544–4554.
Wong, S. N., Li, S., Low, K. H., Chan, H. W., Zhang, X., Chow, S., Hui, B., Chow, P. C. & Chow, S. F. (2024). *Int. J. Pharm.* **653**, 123896.
Zakharychev, V. V. & Martsynkevich, A. M. (2024). *Adv. Agrochem.* **4**, 30–48.
Zeng, W., Wang, X., Kong, X., Li, Y. & Zhang, Y. (2023). *J. Mol. Struct.* **1279**, 135017.
Zhao, Y. & Truhlar, D. G. (2008). *Acc. Chem. Res.* **41**, 157–167.
Zhurko, G. A. (2026). *Chemcraft – graphical software for visualization of quantum chemistry computations*. https://www.chemcraftprog.com.

supporting information

Acta Cryst. (2026). C**82**, 267-276 [https://doi.org/10.1107/S2053229626004882]

Structure and intermolecular interactions of the rare amide–pyridine synthon: a cocrystal of nicotinamide and 2-chloro-3-hydroxypyridine

Oluwatoyin Akerele and Andreas Lemmerer

Computing details

Nicotinamide–2-chloropyridin-3-ol (1/1)

Crystal data

$C_6H_6N_2O·C_5H_4ClNO$
$M_r = 251.67$
Monoclinic, $P2_1/n$
$a = 8.0095$ (3) Å
$b = 6.6434$ (2) Å
$c = 20.6585$ (6) Å
$\beta = 92.563$ (1)°
$V = 1098.15$ (6) Å^3
$Z = 4$
$F(000) = 520$
$D_x = 1.522$ Mg m^{-3}
Mo $K\alpha$ radiation, $\lambda = 0.71073$ Å
Cell parameters from 8491 reflections
$\theta = 2.8$–28.2°
$\mu = 0.34$ mm^{-1}
$T = 173$ K
Block, colourless
0.20 × 0.15 × 0.09 mm

Data collection

Bruker APEXII CCD diffractometer
φ and ω scans
19834 measured reflections
2745 independent reflections
2461 reflections with $I > 2\sigma(I)$
$R_{int} = 0.041$
$\theta_{max} = 28.5°$, $\theta_{min} = 2.8°$
$h = -10 \rightarrow 10$
$k = -8 \rightarrow 8$
$l = -27 \rightarrow 27$

Refinement

Refinement on F^2
Least-squares matrix: full
$R[F^2 > 2\sigma(F^2)] = 0.032$
$wR(F^2) = 0.091$
$S = 1.06$
2745 reflections
155 parameters
0 restraints
Hydrogen site location: inferred from neighbouring sites
H-atom parameters constrained
$w = 1/[\sigma^2(F_o^2) + (0.0474P)^2 + 0.3036P]$ where $P = (F_o^2 + 2F_c^2)/3$
$(\Delta/\sigma)_{max} = 0.001$
$\Delta\rho_{max} = 0.33$ e Å^{-3}
$\Delta\rho_{min} = -0.23$ e Å^{-3}

Special details

Geometry. All esds (except the esd in the dihedral angle between two l.s. planes) are estimated using the full covariance matrix. The cell esds are taken into account individually in the estimation of esds in distances, angles and torsion angles; correlations between esds in cell parameters are only used when they are defined by crystal symmetry. An approximate (isotropic) treatment of cell esds is used for estimating esds involving l.s. planes.

Fractional atomic coordinates and isotropic or equivalent isotropic displacement parameters (Å²)

	x	*y*	*z*	U_{iso}*/U_{eq}
C1	0.91386 (14)	0.40306 (17)	0.34868 (5)	0.0232 (2)
C2	0.99814 (14)	0.39376 (17)	0.29070 (5)	0.0235 (2)
C3	0.98088 (14)	0.56103 (18)	0.25010 (5)	0.0267 (2)
H3	1.034587	0.564410	0.210031	0.032*
C4	0.88468 (15)	0.72178 (18)	0.26887 (6)	0.0283 (2)
H4	0.871779	0.836738	0.241753	0.034*
C5	0.80744 (15)	0.71427 (18)	0.32728 (6)	0.0282 (2)
H5	0.741706	0.825759	0.339603	0.034*
Cl1	0.92892 (4)	0.19616 (4)	0.39996 (2)	0.03404 (11)
N1	0.82173 (12)	0.55539 (15)	0.36730 (4)	0.0259 (2)
O1	1.08765 (12)	0.22962 (14)	0.27814 (4)	0.0324 (2)
H1	1.107768	0.227032	0.238590	0.049*
C6	0.61938 (14)	0.49158 (17)	0.62830 (5)	0.0247 (2)
H6	0.548746	0.579455	0.650902	0.030*
C7	0.66839 (13)	0.54918 (16)	0.56739 (5)	0.0220 (2)
C8	0.60572 (14)	0.74619 (17)	0.54085 (5)	0.0238 (2)
C9	0.77168 (15)	0.41948 (18)	0.53499 (5)	0.0280 (2)
H9	0.808497	0.453393	0.493287	0.034*
C10	0.82039 (16)	0.24018 (19)	0.56414 (6)	0.0306 (3)
H10	0.890217	0.148876	0.542526	0.037*
C11	0.76634 (15)	0.19536 (17)	0.62507 (6)	0.0267 (2)
H11	0.801326	0.072751	0.645083	0.032*
N2	0.66666 (13)	0.31842 (14)	0.65679 (5)	0.0259 (2)
N3	0.64648 (13)	0.79454 (15)	0.48073 (5)	0.0286 (2)
H3A	0.611928	0.909029	0.463403	0.034*
H3B	0.707859	0.711870	0.458502	0.034*
O2	0.52020 (11)	0.85563 (13)	0.57435 (4)	0.0319 (2)

Atomic displacement parameters (Å²)

	U^{11}	U^{22}	U^{33}	U^{12}	U^{13}	U^{23}
C1	0.0283 (5)	0.0211 (5)	0.0202 (5)	0.0004 (4)	0.0026 (4)	0.0002 (4)
C2	0.0271 (5)	0.0225 (5)	0.0212 (5)	0.0002 (4)	0.0030 (4)	−0.0021 (4)
C3	0.0293 (5)	0.0287 (6)	0.0224 (5)	−0.0007 (4)	0.0042 (4)	0.0022 (4)
C4	0.0317 (6)	0.0263 (6)	0.0270 (5)	0.0018 (5)	0.0017 (4)	0.0066 (4)
C5	0.0304 (6)	0.0255 (6)	0.0289 (6)	0.0060 (4)	0.0027 (4)	0.0019 (4)
Cl1	0.0531 (2)	0.02373 (16)	0.02636 (16)	0.00849 (12)	0.01378 (13)	0.00498 (10)
N1	0.0294 (5)	0.0254 (5)	0.0234 (4)	0.0033 (4)	0.0048 (3)	0.0000 (4)
O1	0.0477 (5)	0.0277 (4)	0.0227 (4)	0.0101 (4)	0.0120 (4)	−0.0002 (3)
C6	0.0281 (5)	0.0230 (5)	0.0234 (5)	0.0010 (4)	0.0058 (4)	−0.0009 (4)
C7	0.0253 (5)	0.0201 (5)	0.0207 (5)	0.0004 (4)	0.0019 (4)	−0.0006 (4)
C8	0.0265 (5)	0.0213 (5)	0.0235 (5)	0.0013 (4)	0.0010 (4)	−0.0006 (4)
C9	0.0360 (6)	0.0262 (6)	0.0225 (5)	0.0058 (5)	0.0080 (4)	0.0025 (4)
C10	0.0398 (6)	0.0263 (6)	0.0263 (5)	0.0095 (5)	0.0088 (5)	0.0010 (5)
C11	0.0326 (6)	0.0223 (5)	0.0253 (5)	0.0008 (4)	0.0022 (4)	0.0024 (4)

N2	0.0318 (5)	0.0236 (5)	0.0227 (4)	−0.0006 (4)	0.0057 (4)	0.0017 (4)
N3	0.0370 (5)	0.0246 (5)	0.0247 (5)	0.0083 (4)	0.0059 (4)	0.0042 (4)
O2	0.0419 (5)	0.0264 (4)	0.0279 (4)	0.0107 (4)	0.0083 (3)	0.0009 (3)

Geometric parameters (Å, º)

C1—C2	1.4024 (15)	C6—N2	1.3391 (14)
C1—Cl1	1.7362 (11)	C7—C8	1.4970 (15)
C1—N1	1.3199 (14)	C7—C9	1.3872 (15)
C2—C3	1.3954 (16)	C8—N3	1.3374 (15)
C2—O1	1.3368 (14)	C8—O2	1.2324 (14)
C3—H3	0.9500	C9—H9	0.9500
C3—C4	1.3824 (16)	C9—C10	1.3831 (16)
C4—H4	0.9500	C10—H10	0.9500
C4—C5	1.3815 (16)	C10—C11	1.3817 (16)
C5—H5	0.9500	C11—H11	0.9500
C5—N1	1.3425 (15)	C11—N2	1.3348 (15)
O1—H1	0.8400	N3—H3A	0.8800
C6—H6	0.9500	N3—H3B	0.8800
C6—C7	1.3886 (14)		
C2—C1—Cl1	117.60 (8)	C6—C7—C8	117.97 (9)
N1—C1—C2	125.41 (10)	C9—C7—C6	117.71 (10)
N1—C1—Cl1	116.98 (8)	C9—C7—C8	124.32 (10)
C3—C2—C1	116.09 (10)	N3—C8—C7	117.28 (10)
O1—C2—C1	118.98 (10)	O2—C8—C7	119.73 (10)
O1—C2—C3	124.93 (10)	O2—C8—N3	123.00 (11)
C2—C3—H3	120.4	C7—C9—H9	120.4
C4—C3—C2	119.21 (10)	C10—C9—C7	119.17 (10)
C4—C3—H3	120.4	C10—C9—H9	120.4
C3—C4—H4	120.2	C9—C10—H10	120.4
C5—C4—C3	119.61 (11)	C11—C10—C9	119.25 (11)
C5—C4—H4	120.2	C11—C10—H10	120.4
C4—C5—H5	118.8	C10—C11—H11	118.9
N1—C5—C4	122.49 (11)	N2—C11—C10	122.26 (11)
N1—C5—H5	118.8	N2—C11—H11	118.9
C1—N1—C5	117.18 (10)	C11—N2—C6	118.30 (10)
C2—O1—H1	109.5	C8—N3—H3A	120.0
C7—C6—H6	118.3	C8—N3—H3B	120.0
N2—C6—H6	118.3	H3A—N3—H3B	120.0
N2—C6—C7	123.31 (10)		
C1—C2—C3—C4	0.10 (16)	C6—C7—C8—O2	3.49 (16)
C2—C1—N1—C5	0.14 (17)	C6—C7—C9—C10	0.27 (17)
C2—C3—C4—C5	−0.02 (18)	C7—C6—N2—C11	0.21 (17)
C3—C4—C5—N1	−0.01 (19)	C7—C9—C10—C11	−0.60 (19)
C4—C5—N1—C1	−0.05 (18)	C8—C7—C9—C10	−179.37 (11)
Cl1—C1—C2—C3	178.87 (8)	C9—C7—C8—N3	3.20 (17)

Cl1—C1—C2—O1	−1.16 (14)	C9—C7—C8—O2	−176.87 (11)
Cl1—C1—N1—C5	−178.90 (9)	C9—C10—C11—N2	0.8 (2)
N1—C1—C2—C3	−0.17 (17)	C10—C11—N2—C6	−0.56 (18)
N1—C1—C2—O1	179.80 (11)	N2—C6—C7—C8	179.60 (10)
O1—C2—C3—C4	−179.87 (11)	N2—C6—C7—C9	−0.07 (17)
C6—C7—C8—N3	−176.45 (10)		

Hydrogen-bond geometry (Å, º)

D—H···*A*	*D*—H	H···*A*	*D*···*A*	*D*—H···*A*
O1—H1···N2	0.84	1.80	2.632	171
N3—H3*A*···O2^{i}	0.88	2.03	2.888	167
N3—H3*B*···N1^{ii}	0.88	2.37	3.206	159

Symmetry codes: (i) −*x*+1, −*y*+2, −*z*+1; (ii) *x*+1/2, −*y*+1/2, *z*−1/2.